Crystal structure of vismodegib, $C_{19}H_{14}Cl_2N_2O_3S$

James A. Kaduk,[1,2,a] Stacy Gates-Rector,[3] and Thomas N. Blanton[3]
[1]*Illinois Institute of Technology, 3101 S. Dearborn St., Chicago, IL 60616, USA*
[2]*North Central College, 131 S. Loomis St., Naperville, IL 60540, USA*
[3]*ICDD, 12 Campus Blvd., Newtown Square, PA 19073-3273, USA*

(Received 24 July 2022; accepted 20 September 2022)

The crystal structure of vismodegib has been solved and refined using synchrotron X-ray powder diffraction data, and optimized using density functional theory techniques. Vismodegib crystallizes in space group $P2_1/a$ (#14) with $a = 16.92070(20)$, $b = 10.20235(4)$, $c = 12.16161(10)$ Å, $\beta = 108.6802(3)°$, $V = 1988.873(9)$ Å^3, and $Z = 4$. The crystal structure consists of corrugated layers of molecules parallel to the *bc*-plane. There is only one classical hydrogen bond in the structure, between the amide nitrogen atom and the N atom of the pyridine ring. Pairs of these hydrogen bonds link the molecules into dimers, with a graph set $R2,2(14) > a > a$. The powder pattern has been submitted to ICDD for inclusion in the Powder Diffraction File™ (PDF®). [doi:10.1017/S0885715622000446]

Key words: vismodegib, Erivedge, crystal structure, Rietveld refinement, density functional theory

I. INTRODUCTION

Vismodegib (sold under the brand name Erivedge) is used to treat unresectable or metastatic basal cell carcinoma. It belongs to a class of medicines referred to as hedgehog pathway inhibitors due to its ability to block the action of a protein that signals cancer cells to multiply (MedLine, 2022). The systematic name (CAS Registry Number 879085-55-9) is 2-chloro-*N*-(4-chloro-3-pyridin-2-ylphenyl)-4-methylsulfonylbenzamide. A two-dimensional molecular diagram is shown in Figure 1.

Vismodegib and processes for its preparation were disclosed in US Patent 7,888,364 B2 (Gunzner *et al.*, 2011; Curis, Inc.). The European Medicines Agency (EMA CHMP, 2013) reports that vismodegib exists primarily in the thermodynamically stable polymorph B. Polymorph A was discovered as the initial crystalline form, but could not be reproduced. Polymorph B is the only one which has been used in clinical development. A single-crystal structure was mentioned, but we found none in the open literature. Forms C and E were observed infrequently during extensive polymorph screening. Parthasaradhi Reddy *et al.* (2014; Hetero Research Foundation) claimed a new polymorph of vismodegib (Form II) and provided powder diffraction data for Form I, which is described as the prior art of the '364 patent. We, therefore, presume that the Hetero Form I corresponds to EMA Form B. The mechanisms of action of vismodegib and clinical trials have been reviewed by Ruiz-Salas *et al.* (2013). This work was carried out as part of a project (Kaduk *et al.*, 2014) to determine the crystal structures of large-volume commercial pharmaceuticals, and include high-quality powder diffraction data for them in the Powder Diffraction File (Gates-Rector and Blanton, 2019).

II. EXPERIMENTAL

Vismodegib was a commercial reagent, purchased from TargetMol (Lot #120202), and was used as-received. The white powder was packed into a 1.5 mm diameter Kapton capillary, and rotated during the measurement at ~50 Hz. The powder pattern was measured at 295 K at beamline 11-BM (Antao *et al.*, 2008; Lee *et al.*, 2008; Wang *et al.*, 2008) of the Advanced Photon Source at Argonne National Laboratory using a wavelength of 0.458968(2) Å from 0.5 to 50° 2θ with a step size of 0.001° and a counting time of 0.1 s per step. The high-resolution powder diffraction data were collected using twelve silicon crystal analyzers that allow for high angular resolution, high precision, and accurate peak positions. A mixture of silicon (NIST SRM 640c) and alumina (NIST SRM 676a; Cline *et al.*, 2011) standard (ratio Al_2O_3:Si = 2:1 by weight) was used to calibrate the instrument and refine the monochromatic wavelength used in the experiment.

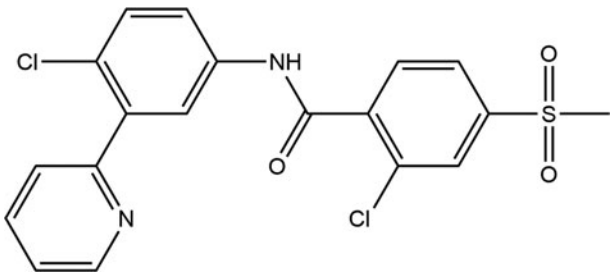

Figure 1. The 2D molecular structure of vismodegib.

[a]Author to whom correspondence should be addressed. Electronic mail: kaduk@polycrystallography.com

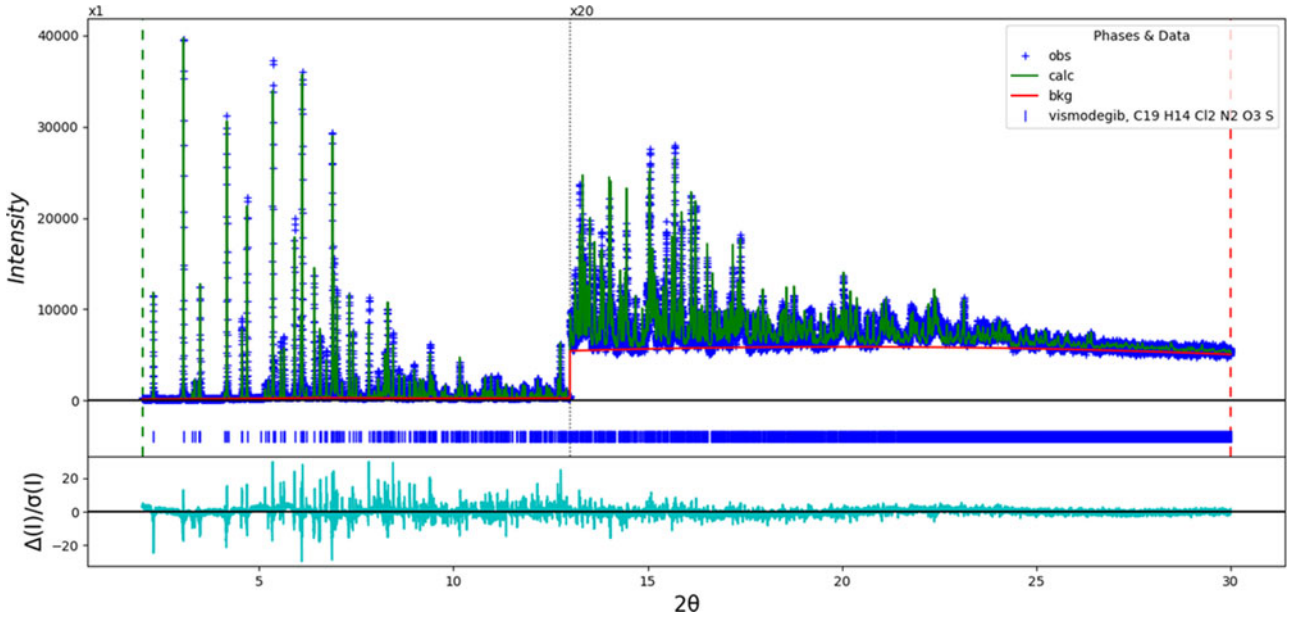

Figure 2. The Rietveld plot for the refinement of vismodegib. The blue crosses represent the observed data points, and the green line is the calculated pattern. The cyan curve is the normalized error plot. The red curve indicates the background. The vertical scale has been multiplied by a factor of 20× for $2\theta > 13.0°$. The row of blue tick marks indicates the calculated reflection positions.

The pattern was indexed using N-TREOR (Altomare *et al.*, 2013) on a primitive monoclinic unit cell with $a =$ 16.8934, $b = 10.1866$, $c = 12.1444$ Å, $\beta = 106.68°$, $V =$ 1979.79 Å^3, and $Z = 4$. A reduced cell search in the Cambridge Structural Database (Groom *et al.*, 2016) yielded 18 hits, but no structures of vismodegib derivatives. The suggested space group was $P2_1/a$, which was confirmed by successful solution and refinement of the structure. The structure was solved by direct methods using EXPO2014 (Altomare *et al.*, 2013). Some atom types had to be reassigned manually, and the hydrogen atoms were added using Materials Studio (Dassault, 2021).

Rietveld refinement was carried out using GSAS-II (Toby and Von Dreele, 2013). Only the 2.0–25.0° portion of the pattern was included in the refinement ($d_{min} = 0.886$ Å). All non-H bond distances and angles (plus the plane of the fused ring system) were subjected to restraints, based on a Mercury/Mogul Geometry Check (Bruno *et al.*, 2004; Sykes *et al.*, 2011). The Mogul average and standard deviation for each quantity were used as the restraint parameters. The restraints contributed 2.1% to the final χ^2. The hydrogen atoms were included in calculated positions, which were recalculated during the refinement using Materials Studio (Dassault, 2021). The U_{iso} of the heavy atoms were grouped by chemical

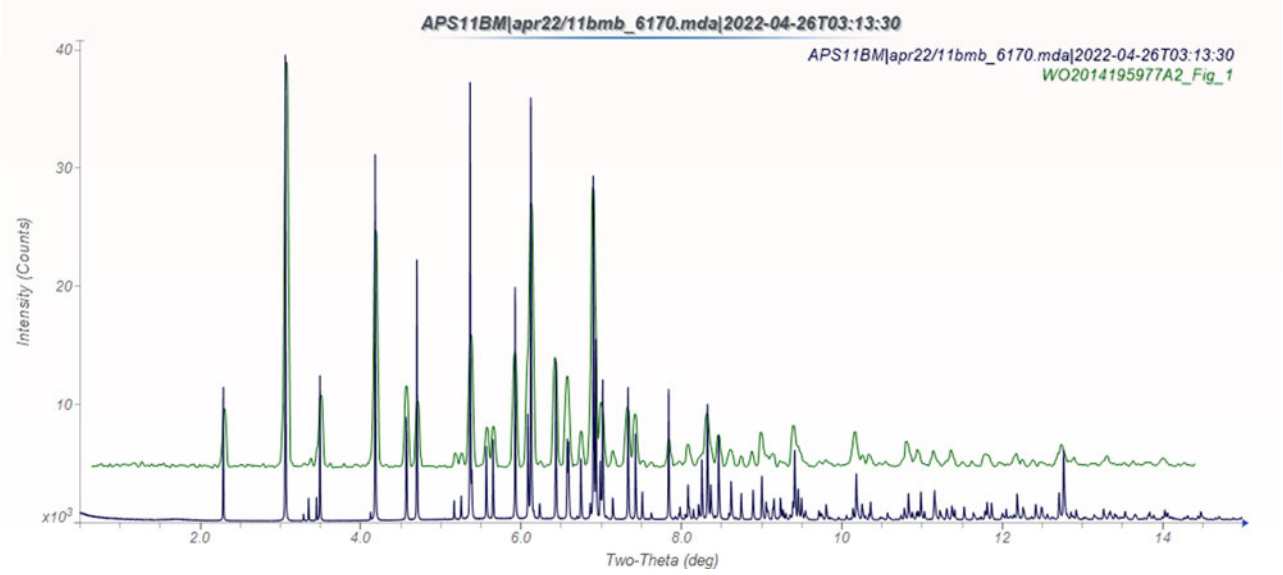

Figure 3. Comparison of the synchrotron pattern of vismodegib (black) to that reported by Parthasaradhi Reddy *et al.* (2014; green) for the prior art Form I, which we identified as the stable Form B. The patent pattern, measured using Cu *Kα* radiation, was digitized using UN-SCAN-IT (Silk Scientific, 2013), and converted to the synchrotron wavelength of 0.458968 Å using JADE Pro (MDI, 2022). Image generated using JADE Pro (MDI, 2022).

https://doi.org/10.1017/S0885715622000446 Published online by Cambridge University Press

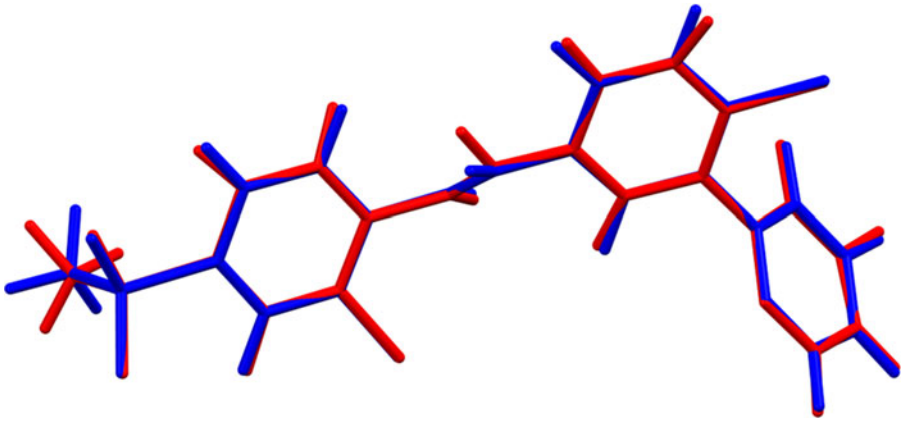

Figure 4. Comparison of the Rietveld-refined (red) and VASP-optimized (blue) structures of vismodegib. The rms Cartesian displacement is 0.055 Å. Image generated using Mercury (Macrae *et al.*, 2020).

similarity. The two Cl atoms were refined anisotropically. The U_{iso} for the H atoms were fixed at 1.3× the U_{iso} of the heavy atoms to which they are attached. The peak profiles were described using the generalized microstrain model. The background was modeled using a 3-term shifted Chebyshev polynomial, and a peak at 6.65° 2θ was used to model the scattering from the Kapton capillary and any amorphous component.

The final refinement of 122 variables using 28 045 observations and 71 restraints yielded the residuals $R_{wp} = 0.1300$ and GOF = 3.27. The largest peak (2.20 Å from C15) and hole (1.94 Å from C19) in the difference Fourier map were 0.50(12) and −0.53(12) eÅ^{-3}, respectively. The largest errors in the difference plot (Figure 2) are in the shapes of many of the strong low-angle peaks, and suggest that the sample may have suffered beam damage during the measurement.

The crystal structure was optimized using VASP (Kresse and Furthmüller, 1996) (fixed experimental unit cell) through the MedeA graphical interface (Materials Design, 2016). The calculation was carried out on 16 2.4 GHz processors (each with 4 GB RAM) of a 64-processor HP Proliant DL580 Generation 7 Linux cluster at North Central College. The calculation used the GGA-PBE functional, a plane wave cutoff energy of 400.0 eV, and a k-point spacing of 0.5 Å^{-1} leading to a 2 × 2 × 2 mesh, and took ∼64.7 h. A single-point density functional calculation (fixed experimental cell) and population analysis were carried out using CRYSTAL17 (Dovesi *et al.*, 2018). The basis sets for the H, C, N, and O atoms in the calculation were those of Gatti *et al.* (1994), and those for S and Cl were those of Peintinger *et al.* (2013). The calculations were run on a 3.5 GHz PC using 8 k-points and the B3LYP functional, and took ∼2.6 h.

III. RESULTS AND DISCUSSION

The synchrotron powder pattern of this study matches the pattern for Form I reported by Parthasaradhi Reddy *et al.* (2014) well enough to conclude that they represent the same material (Figure 3), corresponding to the thermodynamically

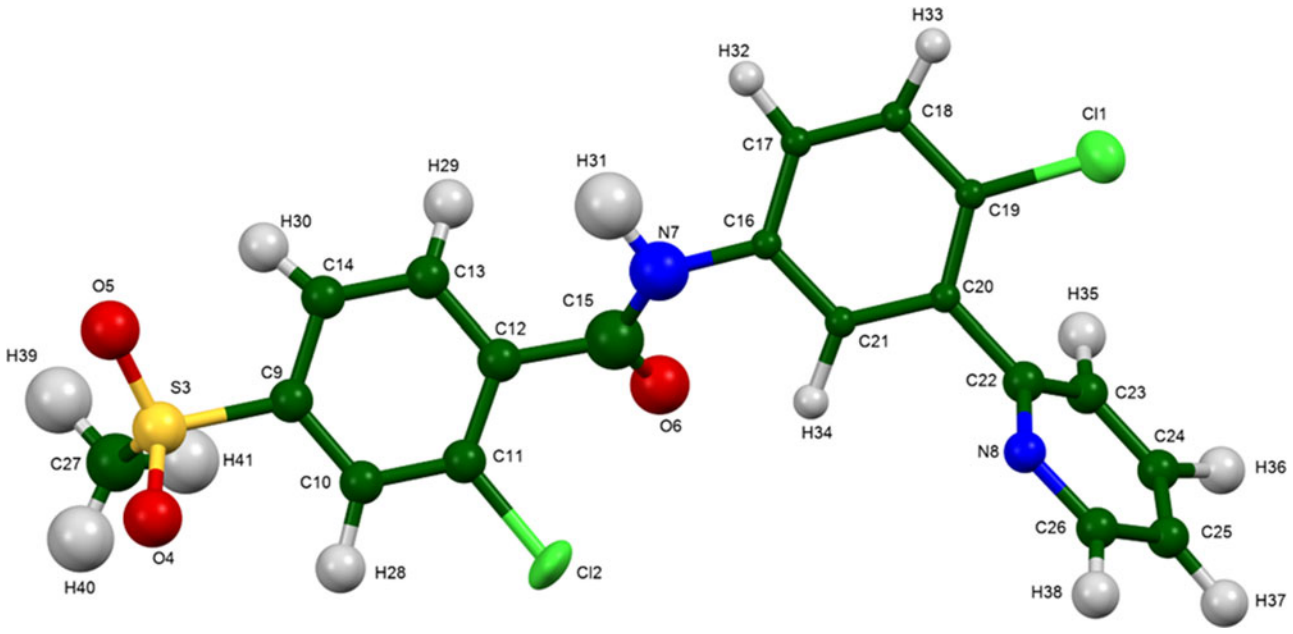

Figure 5. The asymmetric unit of vismodegib, with the atom numbering. The atoms are represented by 50% probability spheroids/ellipsoids. Image generated using Mercury (Macrae *et al.*, 2020).

https://doi.org/10.1017/S0885715622000446 Published online by Cambridge University Press

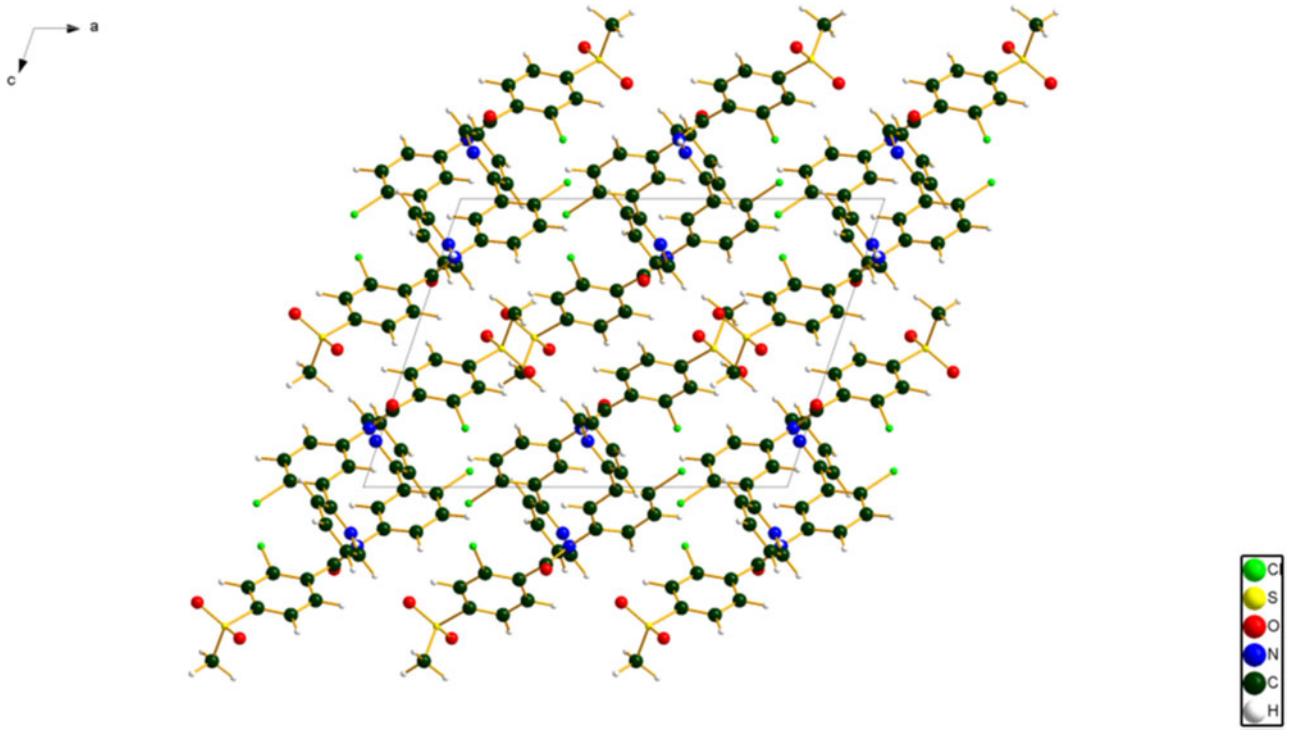

Figure 6. The crystal structure of vismodegib, viewed down the *b*-axis. Image generated using Diamond (Crystal Impact, 2022).

TABLE I. Hydrogen bonds (CRYSTAL17) in vismodegib.

H-Bond	D-H (Å)	H···A (Å)	D···A (Å)	D-H···A (°)	Overlap (*e*)
N7–H31···N8	1.054	1.815	2.861	171.0	0.086
C17–H32···O4	1.091	2.460	3.438	148.6	0.020
C27–H41···O5	1.098	2.419	3.509	171.3	0.018
C27–H39···O6	1.098	2.532	3.570	157.3	0.017
C26–H38···O4	1.092	2.409	3.391	148.7	0.016
C13–H29···O4	1.092	2.715	3.784	166.3	0.014
C27–H40···Cl2	1.099	2.656	3.727	164.7	0.020
C25–H35···Cl2	1.091	2.973	3.941	153.7	0.013

stable Form B of vismodegib. The root-mean-square (rms) Cartesian displacement between the non-H atoms in the Rietveld-refined and DFT-optimized structures is only 0.055 Å (Figure 4), and the maximum difference is 0.118 Å. The excellent agreement is strong evidence that the structure is correct (van de Streek and Neumann, 2014). This discussion concentrates on the DFT-optimized structure. The asymmetric unit (with atom numbering) is illustrated in Figure 5. The best view of the crystal structure is down the *b*-axis (Figure 6). The crystal structure consists of corrugated layers of molecules parallel to the *bc*-plane.

All of the bond distances and bond angles fall within the normal ranges indicated by a Mercury/Mogul Geometry check (Macrae *et al.*, 2020). The torsion angles involving rotation about the C20–C22 bond are flagged as unusual. These represent the orientation of the pyridine ring with respect to one of the chlorinated phenyl rings, and indicate that the overall conformation of the molecule in the solid state is unusual.

Quantum chemical geometry optimization of the vismodegib molecule (DFT/B3LYP/6-31G*/water) using Spartan '18 (Wavefunction, 2020) indicated that the observed conformation is 5.8 kcal mol^{-1} higher in energy than the local minimum, which has more-normal torsion angles about the C20–C22 bond and a different orientation of the methylsulfone group. A conformational analysis (MMFF force field) indicates that the minimum-energy conformation is 1.9 kcal mol^{-1} lower in energy, with further differences in the C20–C22 rotation and the different orientation of the methylsulfone group. Intermolecular interactions seem to be important in determining the solid-state conformation.

Analysis of the contributions to the total crystal energy of the structure using the Forcite module of Materials Studio (Dassault, 2021) suggests that the intramolecular deformation energy is dominated by angle distortion terms. The intermolecular energy is dominated by electrostatic attractions, which in this force field analysis include hydrogen bonds. The hydrogen bonds are better analyzed using the results of the DFT calculation.

There is only one classical hydrogen bond in the structure (Table I), N7–H31···N8. This is between the amide nitrogen atom and the N atom of the pyridine ring. Pairs of these hydrogen bonds link the molecules into dimers, with a graph set (Etter, 1990; Bernstein *et al.*, 1995; Shields *et al.*, 2000) *R2,2(14)>a > a* (Figure 7). Five C–H···O and two C–H···Cl hydrogen bonds also contribute to the lattice energy.

The volume enclosed by the Hirshfeld surface of vismodegib (Figure 8; Hirshfeld, 1977; Turner *et al.*, 2017) is 478.87 Å^3, 96.31% of 1/4 the unit cell volume. The packing density is thus fairly dense. The only significant-close contacts (red in Figure 8) involve the hydrogen bonds. The volume/non-hydrogen atom is larger than normal at 18.4 Å^3, reflecting the presence of the two Cl atoms.

The Bravais–Friedel–Donnay–Harker (Bravais, 1866; Friedel, 1907; Donnay and Harker, 1937) morphology suggests that we might expect blocky morphology for vismodegib, with {001} as principal faces. A second-order spherical harmonic

https://doi.org/10.1017/S0885715622000446 Published online by Cambridge University Press

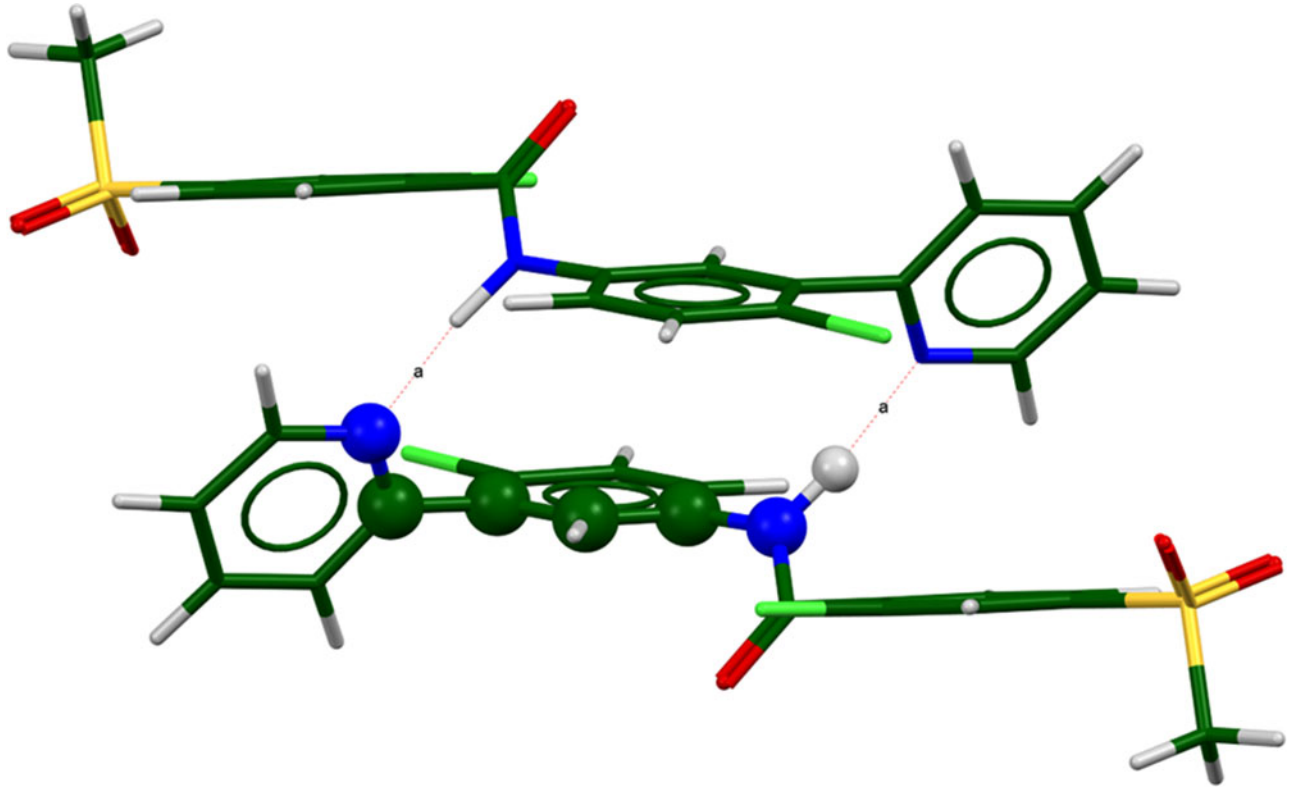

Figure 7. The hydrogen-bonded dimers of vismodegib, linked by two strong N–H···N hydrogen bonds. Image generated using Mercury (Macrae *et al.*, 2020).

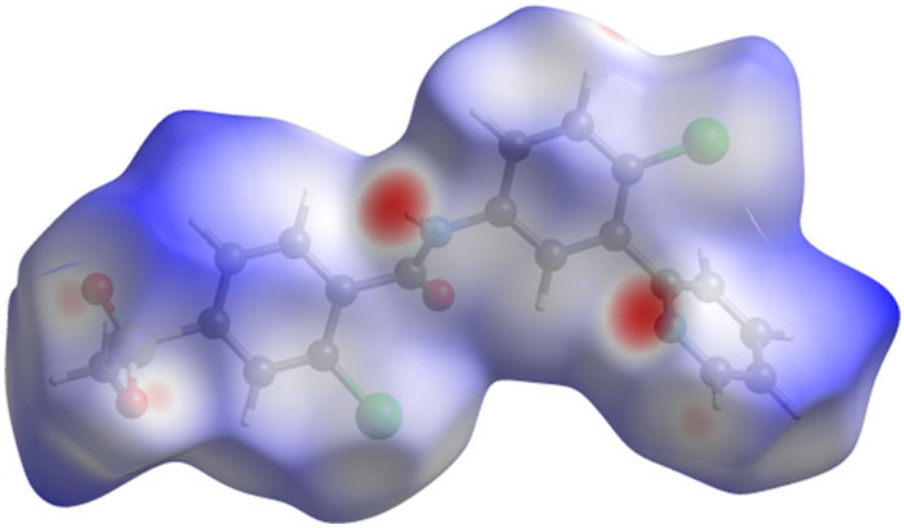

Figure 8. The Hirshfeld surface of vismodegib. Intermolecular contacts longer than the sums of the van der Waals radii are colored blue, and contacts shorter than the sums of the radii are colored red. Contacts equal to the sums of radii are white. Image generated using CrystalExplorer (Turner *et al.*, 2017).

preferred orientation model was included in the refinement. The texture index was 1.018(0), indicating that preferred orientation was not significant for this rotated capillary specimen. The powder pattern of vismodegib from this synchrotron data set has been submitted to ICDD for inclusion in the Powder Diffraction File.

IV. DEPOSITED DATA

The Crystallographic Information Framework (CIF) files containing the results of the Rietveld refinement (including the raw data) and the DFT geometry optimization were deposited with the ICDD. The data can be requested at pdj@icdd.com.

ACKNOWLEDGEMENTS

The use of the Advanced Photon Source at Argonne National Laboratory was supported by the U.S. Department of Energy, Office of Science, Office of Basic Energy Sciences, under Contract No. DE-AC02-06CH11357. This work was partially supported by the International Centre for

https://doi.org/10.1017/S0885715622000446 Published online by Cambridge University Press

Diffraction Data. We thank Lynn Ribaud and Saul Lapidus for their assistance in the data collection.

CONFLICT OF INTEREST

The authors have no conflicts of interest to declare.

Altomare, A., C. Cuocci, C. Giacovazzo, A. Moliterni, R. Rizzi, N. Corriero, and A. Falcicchio. 2013. "EXPO2013: A Kit of Tools for Phasing Crystal Structures from Powder Data." *Journal of Applied Crystallography* 46:1231–35.

Antao, S. M., I. Hassan, J. Wang, P. L. Lee, and B. H. Toby. 2008. "State-of-the-art High-Resolution Powder X-ray Diffraction (HRPXRD) Illustrated with Rietveld Refinement of Quartz, Sodalite, Tremolite, and Meionite." *Canadian Mineralogist* 46:1501–9.

Bernstein, J., R. E. Davis, L. Shimoni, and N. L. Chang. 1995. "Patterns in Hydrogen Bonding: Functionality and Graph Set Analysis in Crystals." *Angewandte Chemie International Edition in English* 34 (15):1555–73.

Bravais, A. 1866. *Etudes Cristallographiques*. Paris: Gauthier Villars.

Bruno, I. J., J. C. Cole, M. Kessler, J. Luo, W. D. S. Motherwell, L. H. Purkis, B. R. Smith, R. Taylor, R. I. Cooper, S. E. Harris, and A. G. Orpen. 2004. "Retrieval of Crystallographically-Derived Molecular Geometry Information." *Journal for Chemical Information and Computer Scientists* 44:2133–44.

Cline, J. P., R. B. Von Dreele, R. Winburn, P. W. Stephens, and J. J. Filliben. 2011. "Addressing the Amorphous Content Issue in Quantitative Phase Analysis: The Certification of NIST Standard Reference Material 676a." *Acta Crystallographica Section A: Foundations of Crystallography* 67 (4):57–367.

Crystal Impact - Dr. H. Putz & Dr. K. Brandenburg. 2022. *Diamond - Crystal and Molecular Structure Visualization*. Bonn, Germany. https://www.crystalimpact.de/diamond.

Dassault Systèmes. 2021. *Materials Studio 2021*. San Diego CA: BIOVIA.

Donnay, J. D. H., and D. Harker. 1937. "A New Law of Crystal Morphology Extending the Law of Bravais." *American Mineralogist* 22:446–7.

Dovesi, R., A. Erba, R. Orlando, C. M. Zicovich-Wilson, B. Civalleri, L. Maschio, M. Rerat, S. Casassa, J. Baima, J. Salustro, and B. Kirtman. 2018. "Quantum-Mechanical Condensed Matter Simulations with CRYSTAL." *WIREs Computational Molecular Science* 8:e1360.

Etter, M. C. 1990. "Encoding and Decoding Hydrogen-Bond Patterns of Organic Compounds." *Accounts of Chemical Research* 23 (4):120–6.

European Medicines Agency Committee for Medicinal Products for Human Use (CHMP). 2013. Assessment report: vismodegib. EMA/297688/2013.

Friedel, G. 1907. "Etudes sur la loi de Bravais." *Bulletin de la Société française de Minéralogie* 30:326–455.

Gates-Rector, S., and T. Blanton. 2019. "The Powder Diffraction File: A Quality Materials Characterization Database." *Powder Diffraction* 39 (4): 352–60.

Gatti, C., V. R. Saunders, and C. Roetti. 1994. "Crystal-Field Effects on the Topological Properties of the Electron-Density in Molecular Crystals - the Case of Urea." *Journal of Chemical Physics* 101:10686–96.

Groom, C. R., I. J. Bruno, M. P. Lightfoot, and S. C. Ward. 2016. "The Cambridge Structural Database." *Acta Crystallographica Section B: Structural Science, Crystal Engineering and Materials* 72:171–9.

Gunzner, J. L., D. Sutherlin, M. S. Stanley, L. Bao, G. M. Castanedo, R. L. Lalonde, S. Wang, M. E. Reynolds, S. J. Savage, K. Malesky, and M. S. Dina. 2011. "Pyridyl Inhibitors of Hedgehog Signalling." United State Patent 7,888,364 B2.

Hirshfeld, F. L. 1977. "Bonded-Atom Fragments for Describing Molecular Charge Densities." *Theoretical Chemistry Accounts* 44:129–38.

Kaduk, J. A., C. E. Crowder, K. Zhong, T. G. Fawcett, and M. R. Suchomel. 2014. "Crystal Structure of Atomoxetine Hydrochloride (Strattera), $C_{17}H_{22}NOCl$." *Powder Diffraction* 29 (3):269–73.

Kresse, G., and J. Furthmüller. 1996. "Efficiency of Ab-Initio Total Energy Calculations for Metals and Semiconductors Using a Plane-Wave Basis Set." *Computational Materials Science* 6:15–50.

Lee, P. L., D. Shu, M. Ramanathan, C. Preissner, J. Wang, M. A. Beno, R. B. Von Dreele, L. Ribaud, C. Kurtz, S. M. Antao, X. Jiao, and B. H. Toby. 2008. "A Twelve-Analyzer Detector System for High-Resolution Powder Diffraction." *Journal of Synchrotron Radiation* 15 (5):427–32.

Macrae, C. F., I. Sovago, S. J. Cottrell, P. T. A. Galek, P. McCabe, E. Pidcock, M. Platings, G. P. Shields, J. S. Stevens, M. Towler, and P. A. Wood. 2020. "*Mercury* 4.0: From Visualization to Design and Prediction." *Journal of Applied Crystallography* 53:226–35.

Materials Design. 2016. *MedeA 2.20.4*. Angel Fire, NM: Materials Design Inc.

MDI. 2022. *JADE Pro version 8.2* (Computer software). Livermore, CA: Materials Data.

Parthasaradhi Reddy, B., K. Rathnakar Reddy, D. Muralidhara Reddy, I. Srinivas Reddy, and B. Vamsi Krishna. 2014. "Novel Polymorphs of Vismodegib." International Patent Application WO 2014/195977 A2.

Peintinger, M. F., D. Vilela Oliveira, and T. Bredow. 2013. "Consistent Gaussian Basis Sets of Triple-Zeta Valence with Polarization quality for Solid-State Calculations." *Journal of Computational Chemistry* 34:451–9.

Ruiz-Salas, V., M. Alegre, A. López-Ferrer, and J. R. López-Ferrer. 2013. "Vismodegib: A Review." *Actas Dermo-Sifiliograficas* 105:744–51.

Shields, G. P., P. R. Raithby, F. H. Allen, and W. S. Motherwell. 2000. "The Assignment and Validation of Metal Oxidation States in the Cambridge Structural Database." *Acta Crystallographica Section B: Structural Science* 56 (3):455–65.

Silk Scientific. 2013. *UN-SCAN-IT 7.0*. Orem, UT: Silk Scientific Corporation.

Sykes, R. A., P. McCabe, F. H. Allen, G. M. Battle, I. J. Bruno, and P. A. Wood. 2011. "New Software for Statistical Analysis of Cambridge Structural Database Data." *Journal of Applied Crystallography* 44:882–6.

Toby, B. H., and R. B. Von Dreele. 2013. "GSAS II: The Genesis of a Modern Open Source all Purpose Crystallography Software Package." *Journal of Applied Crystallography* 46:544–9.

Turner, M. J., J. J. McKinnon, S. K. Wolff, D. J. Grimwood, P. R. Spackman, D. Jayatilaka, and M. A. Spackman. 2017. *CrystalExplorer17*. University of Western Australia. http://hirshfeldsurface.net.

van de Streek, J., and M. A. Neumann. 2014. "Validation of Molecular Crystal Structures from Powder Diffraction Data with Dispersion-Corrected Density Functional Theory (DFT-D)." *Acta Crystallographica Section B: Structural Science, Crystal Engineering and Materials* 70 (6):1020–32.

Vismodegib: MedlinePlus Drug. Accessed July 18, 2022. https://medlineplus.gov/druginfo/meds/a612010.html

Wang, J., B. H. Toby, P. L. Lee, L. Ribaud, S. M. Antao, C. Kurtz, M. Ramanathan, R. B. Von Dreele, and M. A. Beno. 2008. "A Dedicated Powder Diffraction Beamline at the Advanced Photon Source: Commissioning and Early Operational Results." *Review of Scientific Instruments* 79:085105.

Wavefunction, Inc. 2020. *Spartan '18 Version 1.4.5*. Irvine, CA: Wavefunction Inc.